Aeroheating Testing of the Mars Sample Return Earth Entry System with Surface Roughness

Jonathan S. Cheatwood,* Christopher O. Johnston,† and Brian R. Hollis‡
NASA Langley Research Center, Hampton, Virginia 23681

The Mars Sample Return Earth Entry System is a mission concept which would be the first NASA entry vehicle to utilize a woven thermal protection system as well as a 52.5-degree sphere-cone forebody geometry. Due to its novel design, historic experimental data sets were insufficient to validate the models used to characterize the expected aerothermal environment. A wind tunnel test campaign was funded by the Mars Sample Return Earth Entry System project in the NASA Langley 20-Inch Mach 6 Air Tunnel to obtain validation data. The December 2023 test entry of this campaign sought to obtain thermographic data to capture the impact of supersonic flow near woven surface roughness elements on convective heating augmentation, which was the largest remaining uncertainty in the aerothermal design of the Earth Entry System. Data obtained were consistent with prior results obtained on identical woven patterns without supersonic flow present at the roughness elements. The presence of supersonic flow did not have a noticeable effect on surface convective heating augmentation. Data were leveraged to support the NASA Mars Sample Return flight program and this data set is valuable for validating computational solutions on roughness-resolved grids.

Nomenclature

C_H	=	Convective Heating Film Coefficient, kg/(m$^2\cdot$ s)
$C_{H,FR}$	=	Fay-Riddell Reference Convective Heating Film Coefficient, kg/(m$^2\cdot$ s)
H	=	Enthalpy, J/kg
H_0	=	Freestream Total Enthalpy, J/kg
H_{300}	=	Wall Enthalpy at 300 K, J/kg
H_{AW}	=	Adiabatic Wall Enthalpy, J/kg
H_W	=	Model Surface Enthalpy, J/kg
k	=	Roughness Height, m
Re_{k+}	=	Roughness Reynolds Number
M_∞	=	Freestream Mach Number
Re_∞	=	Freestream Unit Reynolds Number, 1/ft
T_∞	=	Freestream Temperature, K
U_∞	=	Freestream Velocity, m/s
ΔH_{tot}	=	Enthalpy Difference, J/kg
μ_w	=	Wall Viscosity, kg/(m $\cdot$ s)
ρ_w	=	Wall Density, kg/m^3
ρ_∞	=	Freestream Density, kg/m^3
τ_w	=	Wall Shear Stress, N/m^2

I. Introduction

The Mars Sample Return (MSR) project is a NASA mission [1] in which a Sample Retrieval Lander (SRL) with a fetch rover will be flown to Mars to retrieve sample tubes on the surface collected by the Mars 2020 rover [2]. The rover will load the samples onto the Mars Ascent Vehicle (MAV), which will then ascend to Martian orbit. NASA is

*Aerospace Engineer, Aerothermodynamics Branch, AIAA Student Member.
†Aerospace Engineer, Aerothermodynamics Branch, AIAA Senior Member.
‡Aerospace Engineer, Aerothermodynamics Branch, AIAA Associate Fellow.

currently reassessing the concept of operations for returning Martian samples to Earth in an effort to reduce the costs and accelerate the schedule. The Earth Entry System (EES) vehicle concept, which was part of the MSR mission, will be discussed, as the vehicle's aerothermal design challenges were the motivation for this research.

After the MAV brought the samples to orbit, the samples would be put on board the EES vehicle and, upon return to Earth, would descend through the Earth's atmosphere, landing in the Utah Test and Training Range (UTTR). The EES vehicle concept studied was a 1.3-meter diameter, 52.5-degree sphere-cone geometry with a 3-D woven Mid-Density Carbon Phenolic (3MDCP) Thermal Protection System (TPS), which is a derivative of the Heatshield for Extreme Entry Environment Technology (HEEET) [3]. Figure 1 contains an artist's concept of the EES vehicle, an image of the nominal surface roughness pattern of the 3MDCP TPS, and an image showing a post arc-jet test scan of a sample of the TPS. Due to strict planetary protection requirements on landing ellipse size, the EES concept did not include a parachute system.

The 52.5-degree sphere-cone geometry of EES would result in a supersonic boundary layer edge, and supersonic flow was predicted to extend down to near the roughness height of the 3MDCP TPS. This differentiates the EES vehicle from missions with other distributed types of roughness in the TPS, such as Orion or or the Mars Science Laboratory [4].

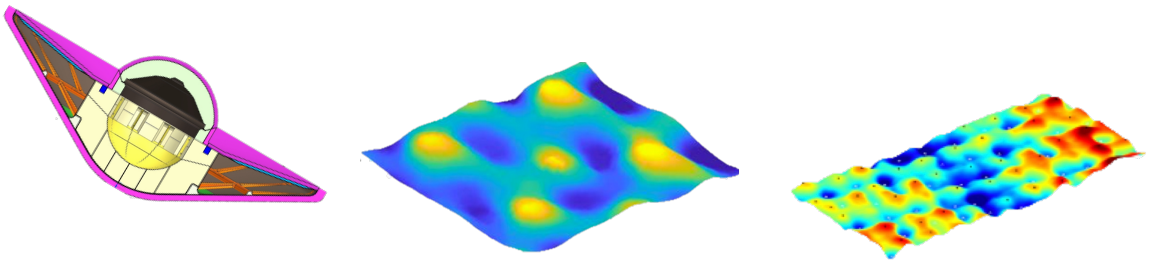

(a) EES Concept **(b) Nominal 3MDCP pattern** **(c) Post arc-jet scan of 3MDCP**

Fig. 1 EES Vehicle Concept and illustrations of the 3MDCP TPS woven roughness pattern.

At the start of the test campaign in early 2023, three specific areas of interest related to aerothermodynamics with high uncertainty, due to insufficient experimental datasets, were identified. These areas were 1) surface heating on a 52.5-degree sphere-cone geometry, 2) surface heating on a 3-D woven roughness pattern, and 3) surface heating on a 3-D woven roughness pattern with supersonic flow present near surface roughness elements. A wind tunnel test campaign at the Langley Aerothermodynamics Laboratory (LAL) 20-Inch Mach 6 Air Tunnel [5] was funded by the MSR-EES project to obtain data to validate the models used to obtain TPS surface heating predictions. The first test entry [6] of this campaign, which will be referred to as test 7078, addressed the first two outlined phenomena and demonstrated that computational predictions post-processed using the Dahm roughness model [7] were in agreement with the experiment and were conservative. The second entry, which will be referred to as test 7087 and was completed in November 2023, aimed to capture data for the remaining item of interest, which is the impact on convective heating augmentation due to the presence of supersonic flow near roughness elements.

This paper presents experimental results obtained from test 7087 and compares them to computational predictions. Data reduction techniques and models used for comparison are also discussed. In addition to the rough surface models, several runs were performed on a smooth 52.5 sphere-cone model to obtain smooth-wall laminar and turbulent data. This smooth-wall data were obtained in support of a EES cone-angle trade study, where 45-degree and 60-degree sphere cones were also being considered for the vehicle.

II. Experimental and Computational Methods

A. Experimental Test Facility and Operating Conditions

The LAL 20-Inch Mach 6 Air Tunnel is a low enthalpy blowdown facility with air as the test gas. The test section is 20.5×20.0 inches, and the wind tunnel model is mounted on a sting and injected into the test section in less than 0.5 seconds. The facility can be operated for up to 15 minutes for a given run, however run times for this study lasted 10 seconds. Nominally, this facility produces perfect-gas freestream flows at Mach numbers of 5.8 to 6.1 and unit Reynolds

numbers of 0.5×10^6 to 8.3×10^6 /ft. A schematic of the LAL Mach 6 facility is shown in Figure 2 and more details of this facility can be found in Refs. [5, 8].

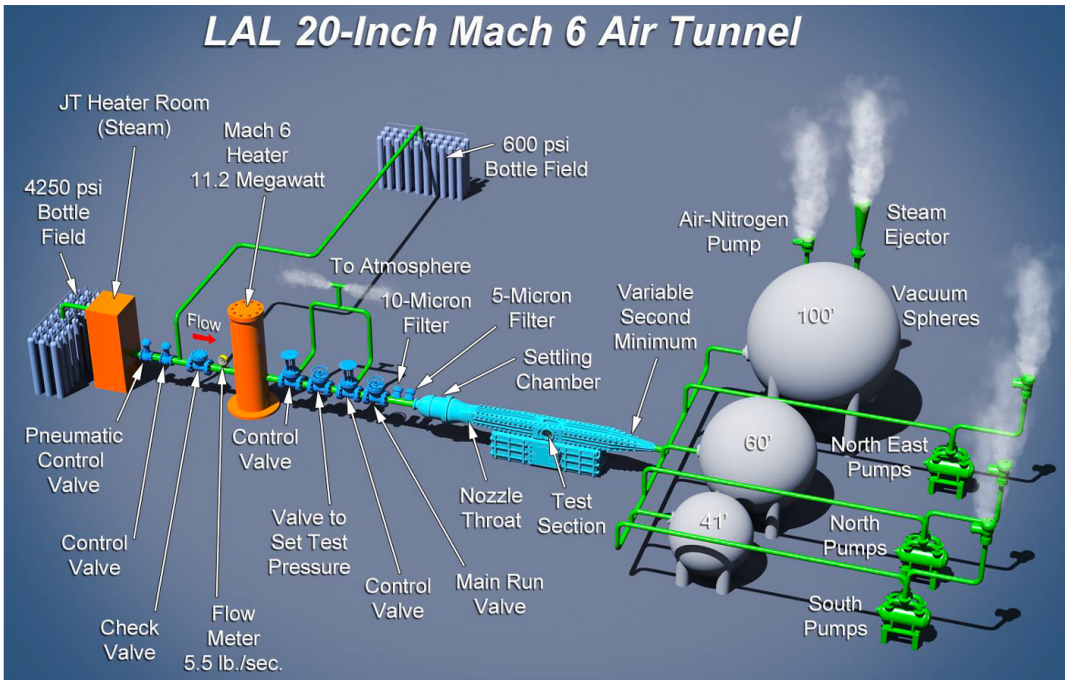

Fig. 2 Schematic of the LAL Mach 6 Hypersonic Facility.

For test 7087, 29 runs were performed over unit Reynolds numbers ranging from $Re_\infty = 2.04 \times 10^6$ to 8.18×10^6 /ft. Mean values for M_∞, U_∞, ρ_∞, T_∞, ΔH_{tot}, and $C_{H,FR}$ for each unit Reynolds condition are tabulated in Table 1. Additionally, Table 1 contains a column indicating which models were run at which conditions. Further information regarding each model can be found in the following subsection.

The enthalpy difference, ΔH_{tot}, is defined as the difference $H_0 - H_{300K}$ between the total enthalpy of the freestream and the wall enthalpy at 300 K, or cold-wall conditions. The reference convective heating film coefficient value, $C_{H,FR}$, is defined as the stagnation convective heating film coefficient value from Fay–Riddell theory [9] for a hemispherical radius at cold-wall conditions, with a radius equal to the nose radius of the wind-tunnel model.

Table 1 Run conditions for the 20-Inch Mach 6 MSR-EES sphere-cone roughness test.

Re_∞, 1/ft	M_∞	T_∞, K	ρ_∞, kg/m^3	U_∞, m/s	ΔH_{tot}, J/kg	$C_{\text{H,FR}}$, kg/(m$^2\cdot$ s)	Models Run
2.04E+06	5.98	62.19	3.16E-02	944.48	2.08E+05	2.54E-01	1, 2
2.45E+06	5.98	61.97	3.78E-02	943.21	2.08E+05	2.78E-01	1, 2
3.02E+06	6.01	62.49	4.68E-02	950.66	2.14E+05	3.12E-01	1, 2, 3T
3.56E+06	6.01	61.74	5.47E-02	945.51	2.08E+05	3.35E-01	1, 2
4.06E+06	6.02	61.54	6.22E-02	944.51	2.07E+05	3.57E-01	1, 2
5.02E+06	6.04	63.11	7.77E-02	959.05	2.22E+05	4.06E-01	1, 2, 3T
5.77E+06	6.04	63.06	8.94E-02	959.39	2.23E+05	4.36E-01	1, 2
6.77E+06	6.04	61.71	1.04E-01	948.25	2.11E+05	4.63E-01	3
7.22E+06	6.05	61.31	1.10E-01	944.93	2.07E+05	4.75E-01	1, 2, 3
7.60E+06	6.05	61.34	1.16E-01	945.30	2.07E+05	4.88E-01	3
8.18E+06	6.04	58.90	1.23E-01	923.34	1.84E+05	4.87E-01	3

B. Wind Tunnel Model Overview

The aim of the MSR-EES test campaign was to measure the impact of roughness augmentation on convective heating for boundary layers with supersonic flow extending down to the roughness height, while matching flight estimates for EES boundary layer parameters. Data measured from these test entries will be used to assess whether the current Dahm model is conservative and whether supersonic flow near elements causes anomalous roughness augmentation. The uncertainty in the impact of this supersonic flow was the primary motivation for test 7087.

Three six-inch diameter cast ceramic models were tested in test 7087. The first two models were identical to two of the models used in test 7078 [6]. These are the largest weave height model, which will be referred to as model 1, and the baseline model, which will be referred to as model 2. Model 1 had a 50% larger weave height than model 2, defined as the peak-to-valley distance of the roughness pattern, and a 50% larger peak-to-peak spacing than model 2. However while the models used in test 7078 were run at $\alpha = 0°$, models 1 and 2 were run at $\alpha = 21°$ in order to generate supersonic flow.

Models 1 and 2 consisted of a 52.5-degree segmented forebody geometry and were mounted to the sting at a 16 degree angle. The forebodies of models 1 and 2 consist of eight separate "panels", half of which are smooth and half of which have woven roughness patterns cast into the model surface. An image of the forebody of model 1 with panels and a trip ring is shown in Figure 3 as well as a side view of the model at angle-of-attack. For the rough panels, the roughness orientation differed between panels A and B. However, for test 7087, only the A panel was studied which contained weave patterns oriented 45 degrees with respect to the oncoming flow.

A trip ring was also cast into models 1 and 2 at the nose-flank junction of two of the smooth panels with the intent of producing turbulence. More information regarding the effectiveness of this trip ring is discussed in Ref [6]. This segmented forebody enabled simultaneous data collection of smooth-wall laminar, smooth-wall turbulent, and rough-wall convective heating data. A representative sinusoidal weave pattern was used for the surface roughness, which was based on post arc-jet test scans of the 3MDCP sample surface, shown in Figure 1. Additional information regarding the woven pattern can be found in Ref [6].

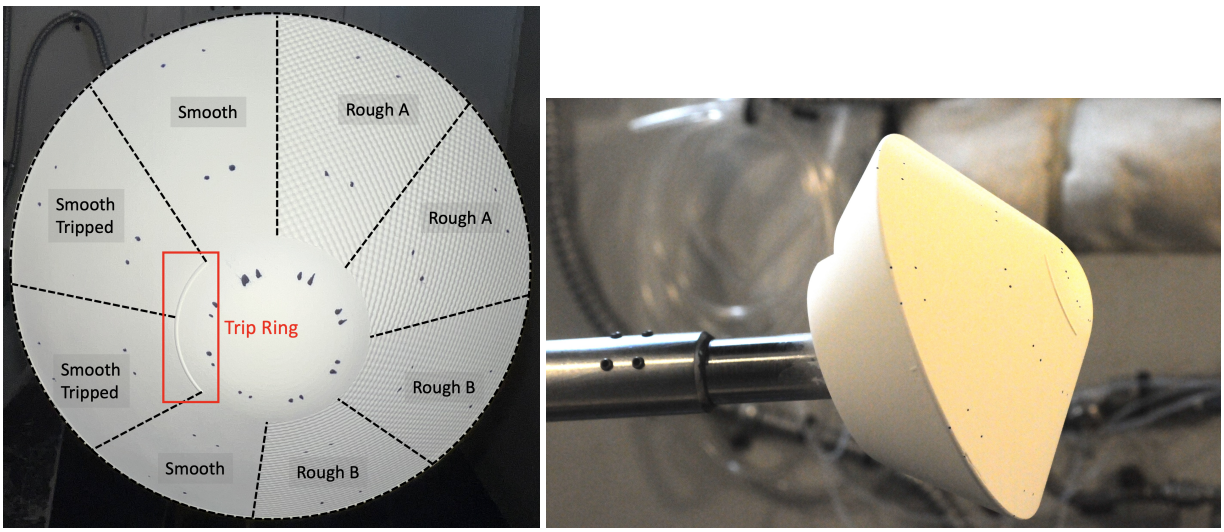

(a) Model 1 with each panel outlined and labeled **(b) Side view of model 1 at angle-of-attack**

Fig. 3 Images of one of the wind tunnel models used in test 7087.

In addition to the sting mounting offset angle, models 1 and 2 were set at 5 degrees angle-of-attack in the tunnel, resulting in the models being run at $\alpha = 21°$. This angle-of-attack was necessary to obtain supersonic flow near the wind tunnel model roughness elements, which would not be seen at wind tunnel conditions if these models were run at $\alpha = 0°$. This is due to the fact that wind tunnel model roughness heights were chosen to match relevant EES roughness Reynolds number values, which were found to be between 35 and 55 for flight. The chosen roughness heights, k, for each model were too small to extend to the supersonic region of the boundary layer unless the models were run at a high angle-of-attack. Figure 4 shows a near-surface Mach number LAURA solution at wind tunnel conditions for a 52.5-degree sphere cone forebody at $\alpha = 21°$. The roughness height of model 2 is indicated by the black dashed line and extends well into the supersonic portion of the boundary later.

The presence of this supersonic flow near roughness elements was predicted to be seen by the EES vehicle even at its nominal $\alpha = 0°$. Models 1 and 2 were run to match this supersonic flow phenomenon, not to match the angle-of-attack at which the EES vehicle would have flown.

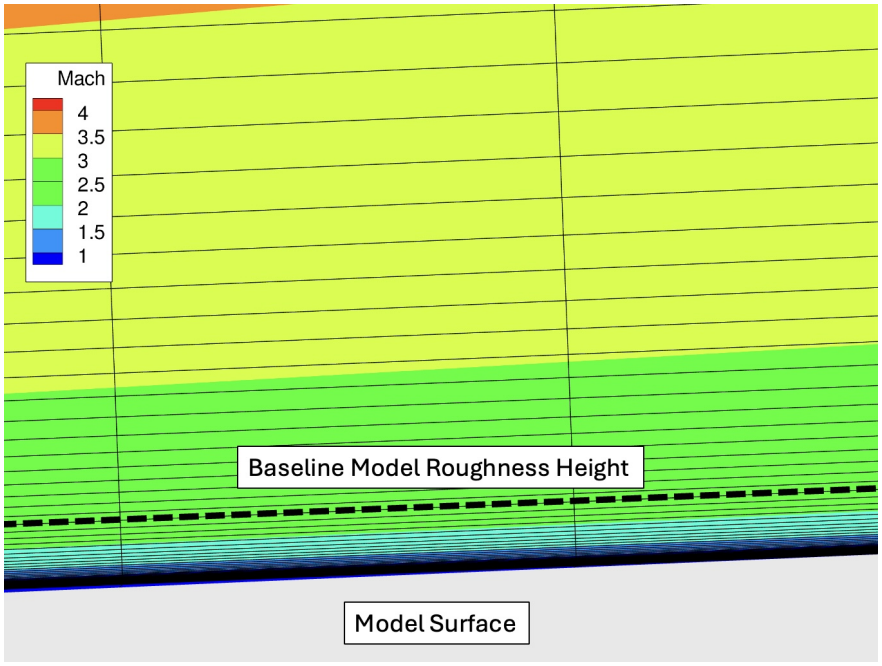

Fig. 4 Near-surface Mach number for a 52.5-degree sphere-cone geometry at $\alpha = 21°$.

The remaining model that was run, model 3, was a smooth-wall 52.5-degree sphere cone run at $\alpha = 0°$. After a Reynolds number sweep was performed, trip tape was added to this model at its nose-flank junction to obtain smooth-wall turbulent heating data. This tripped model will be referred to as model 3T.

C. Phosphor Thermography Data Acquisition Method

Data were measured using the two-color, relative-intensity, global phosphor thermography method [10]. For this method, the model is illuminated by ultraviolet (UV) lights during a wind tunnel run that induce temperature-dependent fluorescence of the phosphor coating that is applied to the surface of each model prior to testing. Intensity images of the model are taken in the tunnel prior to the run, referred to as the Prerun image, and then are taken during the run at a rate of 30 frames per second. Images are captured using a three-color, charge-coupled device camera. The intensity data are converted to temperature using calibrations of the phosphor system prior to testing. The temperature data are processed to determine global surface heat transfer rates. Phosphor Prerun and run intensity images for a run with a unit Reynolds number of 5.02×10^6 /ft are shown in Figure 5.

D. Data Reduction Methods

For standard data reduction, phosphor thermography data are processed using the Imaging for Hypersonic Experimental Aeroheating Testing (IHEAT) code [11] using a technique known as the step-method. For this method, global C_H values are determined by assuming a step function in the convective heating film coefficient from the Prerun temperature to the run temperature. The heating results are typically presented in terms of $C_H/C_{H,FR}$, where C_H is defined in Eq 1.

$$C_H = q/(H_{AW} - H_w) \simeq q/(H_0 - H_w) \tag{1}$$

For calculating the convective heating film coefficient, it is assumed that, for a blunt wind tunnel model, the adiabatic wall enthalpy H_{AW} is equal to the tunnel freestream total enthalpy, H_0. This definition provides a theoretically near-constant value of C_H over the course of a run.

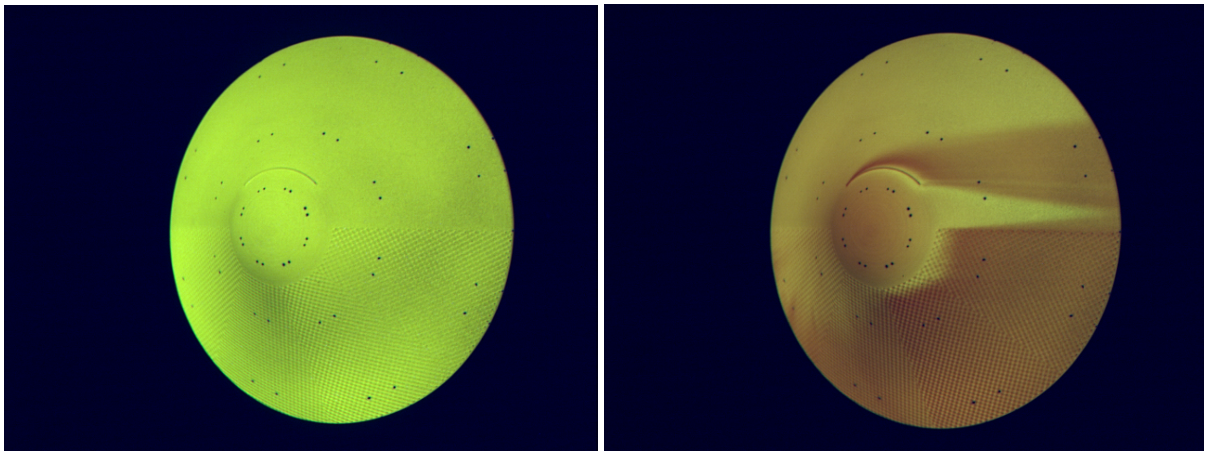

(a) Prerun phosphor intensity image **(b) Frame 120 phosphor intensity image**

Fig. 5 Intensity images of the larger weave model at a condition of $Re_\infty = 5.02 \times 10^6$ /ft.

For test 7087, phosphor data were reduced using a new method, known as the Patch Integral Method (PIM) [12], in addition to IHEAT in order to obtain comparison and validation data for this new method. PIM is currently an experimental code being developed at NASA Langley to be a higher-fidelity successor to the step-method. The main improvements that PIM offers are numerical one-dimensional heat conduction analysis capabilities and the removal of the step heating approximation. Additionally, PIM models the exact variable thermal properties, while the step method uses approximate, constant thermal properties to obtain surface heating.

The standard PIM data reduction workflow is as follows: 1) the Prerun image is treated as an initial condition, 2) the gap in temperature data between the Prerun image and the first run image due to lack of data during model injection is "patched", 3) the temperature data are filtered both spatially and temporally, 4) the one-dimensional heat conduction equation is solved using a finite-difference Crank-Nicolson Method [13] to obtain heat flux, and 6) heating data are mapped to the model geometry to enable direct comparison to CFD results. The heat flux calculated with PIM is used in Eq 1 to obtain C_H.

Fiducial marks were added to the model surfaces to enable data mapping. PIM contains an affine transformation mapping algorithm [14], which was used to map data onto a smooth 52.5-degree sphere-cone forebody geometry, as well as a Radial Basis Function (RBF) mapping algorithm [15]. The fiducial locations chosen and the subsequent mapped data using the affine transformation algorithm are shown in Figure 6

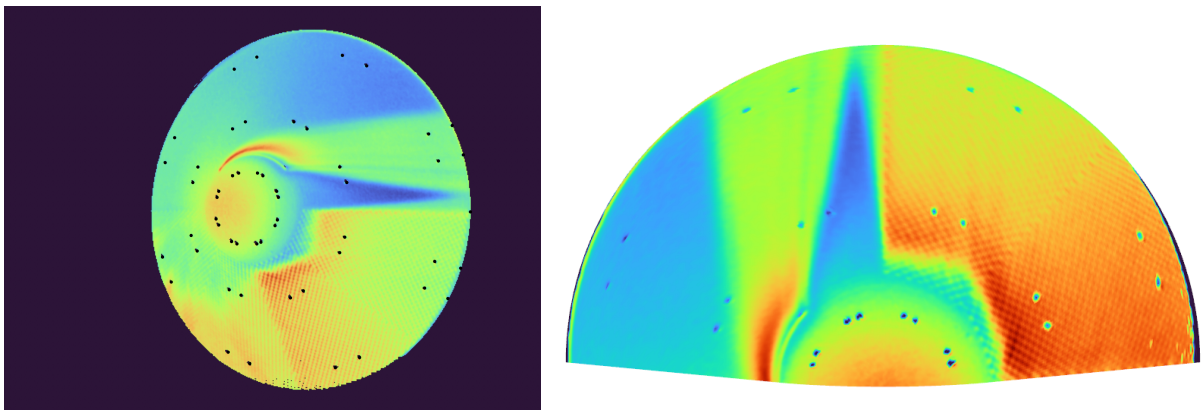

(a) Fiducials chosen for mapping **(b) Mapped PIM heating data**

Fig. 6 PIM heating images for sphere-cone roughness models.

E. Experimental Uncertainty

The experimental uncertainty for convective heat transfer measurements on a smooth, blunt-body geometry model in the 20-Inch Mach 6 Air Tunnel is quantified as a function of net uncertainties resulting from the data acquisition method (10% using the step-method), flow quality and test-condition repeatability (5%), and the accuracy of the 3-D mapping process (10%), which results in an overall root-sum-squared value of 15%. The woven surface roughness patterns are assumed to introduce additional uncertainties due to 1) the tight curvature of the weave elements resulting in multidimensional conduction, which is not modeled by the reduction technique in IHEAT or PIM, 2) insufficient spatial resolution of the weave peaks and valleys due to fixed resolution of the data acquisition system, and 3) lack of illumination of the weave pattern valleys for image regions in which the surface of the model is not normal to the camera system. These rough-wall uncertainties are estimated to be in the 10–20% range, which, when combined with the smooth-wall uncertainty, results in a total experimental uncertainty in convective heat transfer measurements on rough blunt-body geometries to be in the 18–25% range, which is in-family with previous surface roughness tests conducted in the LAL 20-Inch Mach 6 Air Tunnel [16].

As PIM is currently a developmental data reduction capability, data shown in this paper reduced with PIM includes the same amount of uncertainty as the step-method, although its actual uncertainty is likely to be lower due to the increased fidelity of its heat transfer solver and more advanced filtering.

F. Rough-Wall Convective Heating Augmentation Methodology

Because of its steep flight path angle, its large size, and its woven TPS, the EES vehicle would have experienced unprecedented levels of roughness augmentation of the turbulent convective heating. The EES vehicle would have been both the first NASA capsule with a 52.5-degree sphere-cone geometry as well as the first NASA capsule to have a woven TPS. From a mission design perspective, it is currently considered prohibitively expensive to perform CFD analysis on full-vehicle grids that accurately resolve roughness elements due to extremely large grid cell count requirements. As a result, current NASA modeling of roughness effects on aeroheating use correlative models based on roughness Reynolds number, Re_{k+}, defined in Eq 2:

$$Re_{k+} = \left(\frac{\tau_w}{\rho_w}\right)^{1/2} \frac{\rho_w}{\mu_w} k \tag{2}$$

For EES vehicle design, the Dahm roughness model was applied as a post-processing step to smooth-wall CFD results to obtain surface convective heating augmentation as a result of surface roughness. The nominal roughness height was determined from post arc-jet samples of the 3MDCP TPS in the Interactive Heating Facility (IHF) [17] at the NASA Ames Research Center. The Dahm roughness model used for the EES design presented in Figure 7 represents the augmentation factor from a given Re_{k+}, and is defined in Eq 3.

$$C_{H,Augmented} = C_H * (0.46 + 0.54 * log(Re_{k+})) \tag{3}$$

In additional to the lack of flight heritage of the capsule forebody geometry and surface roughness pattern, no NASA experimental aeroheating data sets were identified to be sufficient to validate the current models for woven roughness. As current models do not directly incorporate the woven surface roughness, correlative models of roughness augmentation effects are used. These models are typically applied to small-scale distributed roughness patterns, such as hexcomb [16] and sandgrain roughness [18], both of which have been studied extensively. However, for the EES vehicle, due to its size and its TPS, the scale of roughness elements relative to the boundary layer is significantly larger than previously studied surface roughnesses, and would result in supersonic flow near roughness elements. Existing experimental data sets do not sufficiently validate computation roughness augmentation models for surface roughness with supersonic flow near roughness elements. As a result of this lack of flight heritage and experimental validation data sets, there is added uncertainty to the aeroheating design environments.

G. Computational Tools

The Langley Aerothermodynamic Upwind Relaxation Algorithm (LAURA) [19] flowfield solver was used to characterize the aerothermal environment of the EES vehicle during entry [20]. Flowfield solutions for wind tunnel conditions were also generated using LAURA. LAURA is a three-dimensional, structured-grid, finite-volume solver that includes perfect-gas and non-equilibrium chemistry options, a variety of turbulence models, ablation, and radiative transport capabilities. Line cut extractions were taken of PIM mapped heating data and were directly compared to

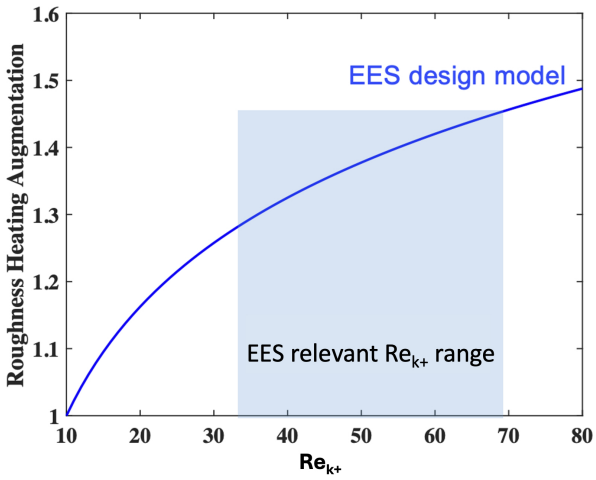

Fig. 7 Dahm roughness model used for EES design.

LAURA solutions in order to assess the accuracy of the modeling of the woven surface roughness as well as to update the convective heating margins used to size the TPS. LAURA solutions for the 52.5-degree sphere-cone geometry were computed on a fourteen-block, three-dimensional, forebody grid with a smooth Outer Mold Line (OML). Freestream conditions for CFD comparison solutions were set to the nominal wind-tunnel conditions for each run, which are outlined in Table 1. For the 52.5-degree sphere-cone solutions at $\alpha = 0°$, an axisymmetric LAURA grid was run to reduce computation time. LAURA solutions can be seen in Figure 8 and block boundaries are outlined in red.

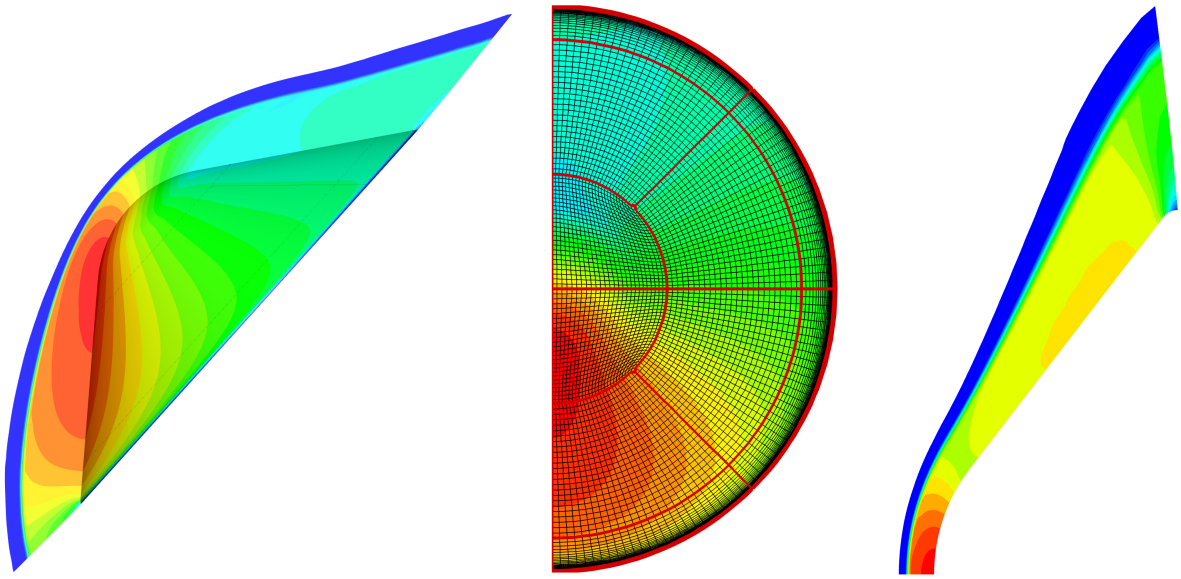

(a) 52.5-degree sphere-cone flowfield pressure **(b) 52.5-degree sphere-cone grid** **(c) Axisymmetric solution**

Fig. 8 LAURA flowfield solutions for 52.5° sphere-cone geometries at a condition of $Re_\infty = 3.56 \times 10^6$ /ft.

The perfect-gas air option was used to generate LAURA solutions. For angle-of-attack comparisons, solutions consisted of laminar, turbulent, and turbulent with roughness augmentation in order to directly compare to data collected from each panel type on the wind tunnel model. The Cebeci–Smith algebraic turbulence model [21] with fully turbulent flow over the entire geometry was used to obtain turbulent heating solutions, and the Dahm roughness model [7] was used to post-process the solutions and determine rough-wall turbulent heating results.

III. Results

A. Angle-of-Attack 52.5-degree Sphere-Cone

The primary objective of test 7087 was to obtain experimental aeroheating data on a woven surface roughness pattern of a 52.5-degree sphere-cone with supersonic flow present near roughness elements. This phenomenon was successfully captured and select data will be presented in this section. As an illustration, Figure 9 contains unmapped line cut extractions taken from heating data on model 1 at a condition of $Re_\infty = 5.02 \times 10^6$, as well as comparisons of the data to the LAURA prediction. Since this figure shows 2-D image data that have not been mapped to the vehicle surface, LAURA results are not directly comparable in this figure, and serve more as a reference for the PIM and step-method comparison. The flank of the sphere-cone was of primary interest for these angle-of-attack runs and comparisons will be focused on these regions of the sphere-cone geometry.

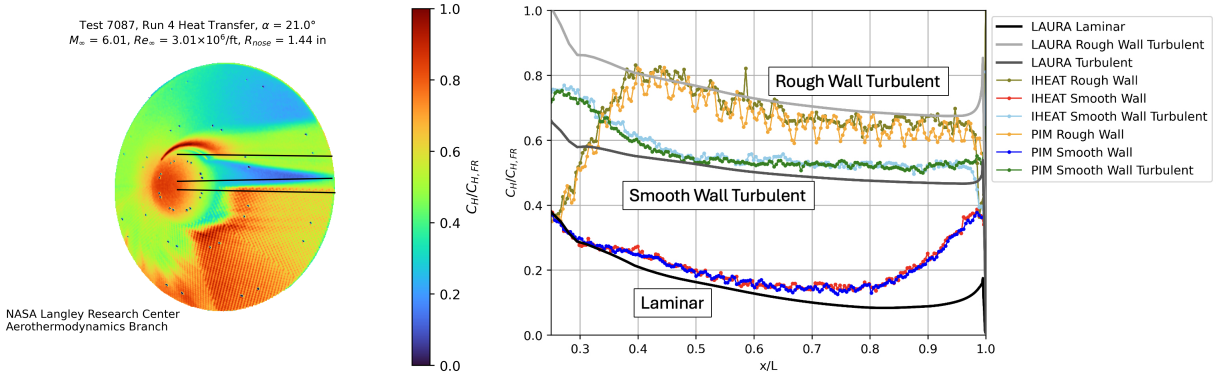

(a) Unmapped heating image with line cuts **(b) Comparison plot of unmapped PIM and IHEAT data with LAURA**

Fig. 9 Unmapped experimental data.

For smooth-wall sections, PIM and IHEAT results are in agreement, however PIM recovers weave peak and valley heating resolution more accurately due to its improved filtering and time integration of surface heating. Line cuts of the laminar and rough-wall sections, which are the bottom two cuts in the left image of Figure 9, were taken for all of the angle-of-attack roughness runs. For each run, heating data were mapped to smooth model geometries and then line cuts were taken and compared to LAURA prediction. Since roughness augmentation is the primary comparison of interest, only rough-wall line cuts will be shown in mapped comparison plots to LAURA. Line cuts were deliberately taken close to the model centerline to make suitable comparisons to LAURA centerline predictions.

Mapped heating data on model 1 at a condition of $Re_\infty = 5.02 \times 10^6$ /ft are plotted with simulation results in Figure 10. The experimental measurements are in agreement with the LAURA predictions, which consist of laminar and turbulent LAURA solution line cuts as well as a "rough-wall turbulent" line cut which is the turbulent solution line cut with the Dahm roughness model applied as a post-processing step. As seen in the image, near the shoulder of the model the smooth-wall heating line cut was impacted by the spreading turbulent flow wedge coming off of the trip ring, and began to trend towards the turbulent heating curve predicted by LAURA. Mapped heating data on model 2 at a condition of $Re_\infty = 7.22 \times 10^6$ /ft are plotted with simulated results in Figure 11. The rough-wall heating measurements obtained on model 2 were consistent with the results on model 1, showing that the Dahm model was conservative for both weave heights, but agreed within 25%.

B. Rough-Wall Heating Aggregate Comparisons

Aggregate comparisons were made across the 16 runs performed on models 1 and 2, similar to test 7078. For this comparison, experimental data were averaged along the rough-wall line cuts from an x/L of 0.65 to an x/L of 0.75. However, only one line cut was considered for these comparisons as the primary focus of this study was to support immediate project needs to assess the accuracy of the Dahm roughness model for a woven roughness pattern, specifically when supersonic flow is present near roughness elements. A more thorough model validation would require comparisons at multiple locations on the model. The comparisons were made far enough downstream to mitigate any impact that the interface between the smooth nose and the rough panel would have on heating, as well as far enough upstream to

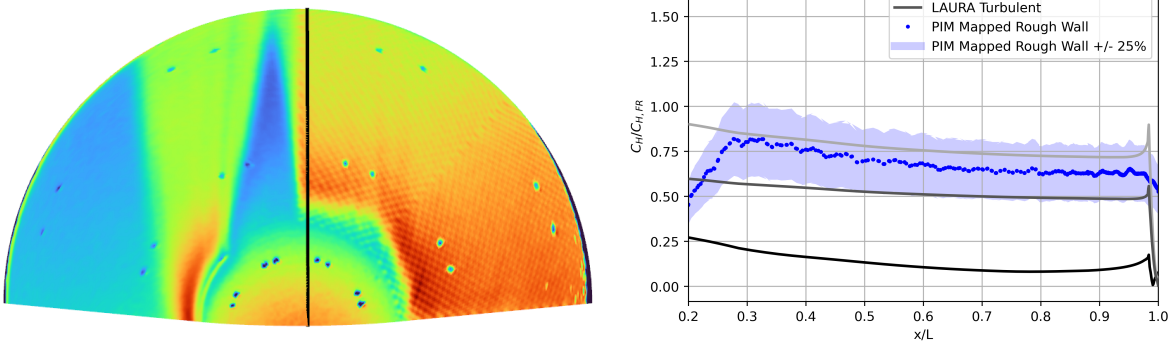

(a) Mapped heating data with line cuts **(b) Mapped heating line cut comparison plot**

Fig. 10 Mapped PIM heating data for model 1 at a condition of $Re_\infty = 5.02 \times 10^6$ /ft.

prevent cross-contamination from adjacent roughness panels. These aggregate comparisons are key to evaluating the accuracy of the current models, as they provide validation across a wide range of Re_{k+} values. Figure 12 shows the comparison performed from test 7078 data and for 13 of the 16 runs of test 7087, as three of the runs did not produce turbulent flow over the rough-wall panel.

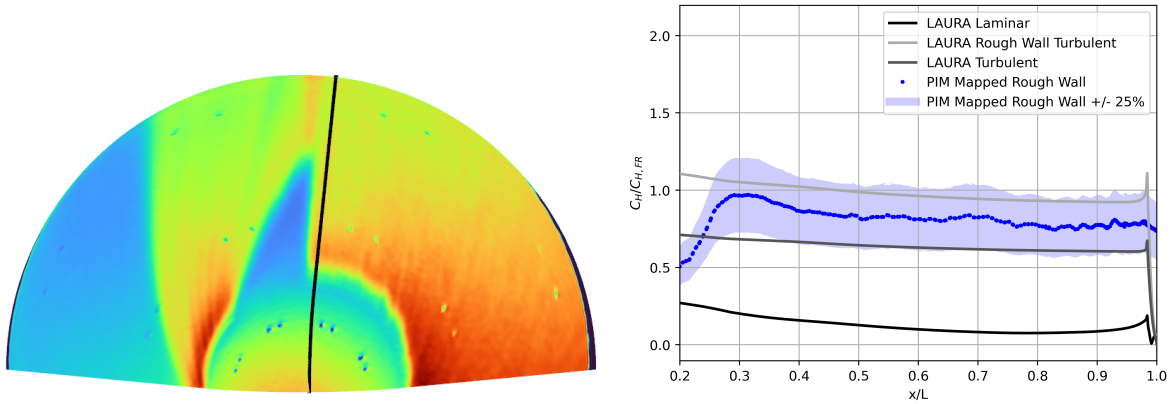

(a) Mapped heating data with line cuts **(b) Mapped heating line cut comparison plot**

Fig. 11 Mapped PIM heating data for model 2 at a condition of $Re_\infty = 7.22 \times 10^6$ /ft.

In Figure 12, experimental measurements reduced by PIM are normalized by simulated predictions to assess the differences between experimental and simulated convective roughness heating augmentation. The measured data are within 20% of the simulation predictions. Apart from the lowest Re_{k+} value, where turbulent heating augmentation is less significant, it was found that the Dahm model used for the MSR-EES project is conservative. This agreement between experimental and simulation results provides confidence in the capability to model woven roughness heating augmentation with existing correlations.

The ratio of measured to simulated heat transfer for the second test campaign seen in Figure 12 for test 7087 is consistent with the comparison performed for test 7078. This valuable result shows the presence of supersonic flow near roughness elements does not have a noticeable impact of heating augmentation. This finding mitigated the largest remaining uncertainty in the design models used to characterize the aerothermal environment for EES, and is an important finding for further understanding woven roughness heating augmentation.

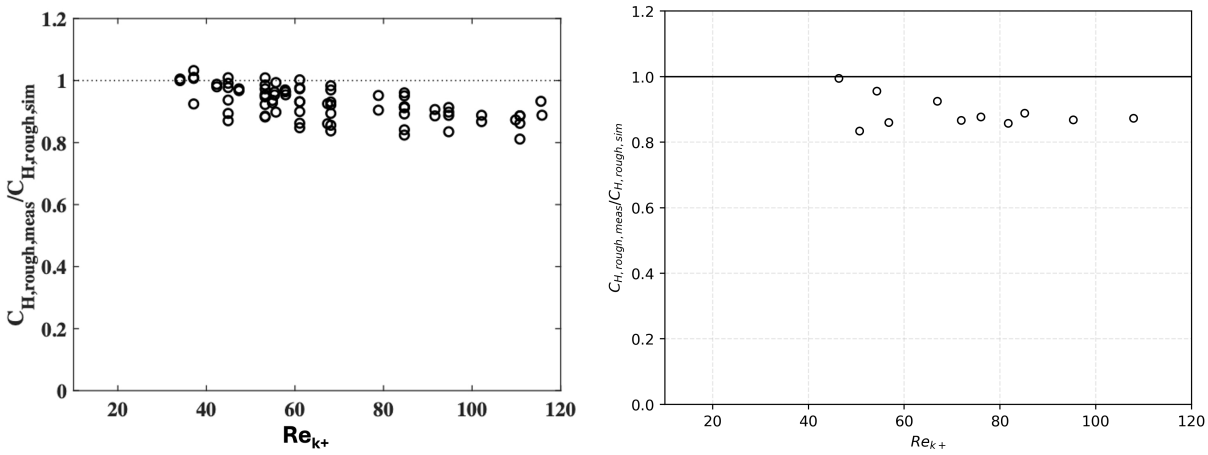

(a) Aggregate comparison for test 7078 [6] **(b) Aggregate comparison for test 7087**

Fig. 12 Aggregate comparison plots of experimental C_H normalized by simulation C_H.

C. Smooth-Wall 52.5-degree Sphere-Cone

In addition to the angle-of-attack rough-wall runs, several runs were performed on model 3 at zero angle-of-attack with the purpose of comparing experimental and CFD smooth-wall results in support of a EES cone-angle trade study effort. A Reynolds number sweep was performed on centerline cuts of model 3. Assuming that the flow remains laminar, $C_H/C_{H,FR}$ across the entire Reynolds number range would be expected to be close to invariant. The Reynolds number sweep results are shown in Figure 13. The experimental data agree with the LAURA laminar predictions and are invariant to Reynolds number.

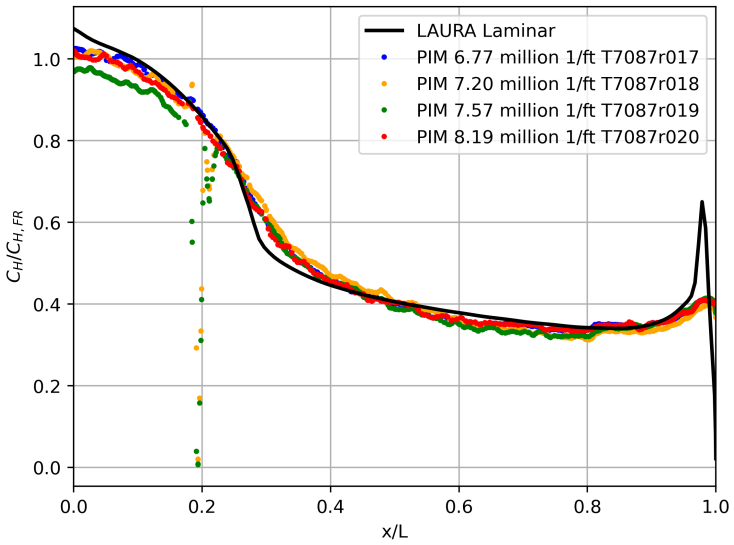

Fig. 13 Reynolds number collapse plot for model 3.

Blunt body smooth-wall, natural transition is not easily attainable at the Mach 6 tunnel operating conditions, so discrete trips were applied at the nose-flank junction of model 3 to obtain smooth-wall turbulent heating data for a 52.5-degree sphere-cone geometry. This tripped model, referred to as model 3T, was used in two runs to obtain turbulent data and the comparisons for a single run for the geometry are shown in Figure 14. The turbulent heating measured on model 3T was also in agreement with the LAURA prediction.

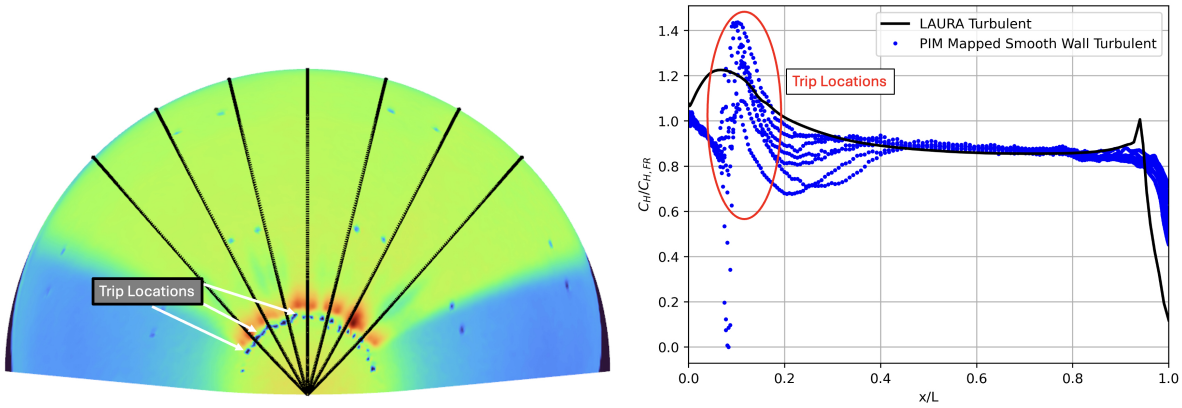

(a) Mapped heating data with line cuts **(b) Mapped heating line cut comparison plot**

Fig. 14 Mapped PIM turbulent heating data and comparison to LAURA for model 3T.

IV. Conclusions

The aim of the MSR-EES test campaign was to measure the impact of roughness augmentation on convective heating for boundary layers with supersonic flow extending down to the roughness height, while matching EES boundary layer quantities, as well as to assess the accuracy of current models of the woven surface roughness heating augmentation.

Overall, the MSR-EES test campaign met its intended goals and successfully produced validation aeroheating data of a 52.5 deg sphere-cone geometry and a woven roughness patterned surface, both with subsonic and supersonic flow near roughness elements. The findings from this campaign were that the Dahm roughness model, while conservative, agreed with experimental rough-wall aeroheating measurements within 20% when applied as a post processing step to LAURA smooth-wall turbulent heating prediction results. The Dahm model was found to be sufficiently applicable to woven roughness patterns. Additionally, it was found that the presence of supersonic flow near roughness elements did not have a significant impact on rough-wall heating augmentation for woven roughness patterns, as aggregate heating comparisons obtained from test 7087 were consistent with results obtained from test 7078.

Several runs were performed which measured smooth-wall laminar and turbulent heating data on a 52.5-degree sphere-cone geometry, and it was found that smooth-wall laminar and turbulent measurements were in agreement with the LAURA prediction. In addition to supporting the development of a proposed MSR-EES concept, the data obtained from test 7087 are generally valuable for research and development toward validating CFD models, as experimental aeroheating measurements on a surface that simulates rough woven TPS are relatively sparse. These data are useful in validation of computational turbulence and correlative roughness models, and can be used to support vehicle design for any future missions that require a woven TPS. These data are also crucial in validating the ongoing development of computational tools and methods to perform economical computations on roughness-resolved grids [22].

Acknowledgments

This work was supported by the NASA Mars Sample Return - Earth Entry System Project within the Mars Sample Return Program of the Science Mission Directorate.

References

[1] Meyer, M. A., Kminek, G., Beaty, D. W., Carrier, B. L., Haltigin, T., Hays, L. E., Agree, C. B., Busemann, H., Cavalazzi, B., Cockell, C. S., et al., "Final Report of the Mars Sample Return Science Planning Group 2 (MSPG2)," , June 2022. https://doi.org/10.1089/ast.2021.0121.

[2] Simon, J., Hickman-Lewis, K., Cohen, B., Mayhew, L., Shuster, D., Debaille, V., Hausrath, E., Weiss, B., Bosak, T., Zorzano, M.-P., et al., "Samples Collected From the Floor of Jezero Crater with the Mars 2020 Perseverance Rover," *Journal of Geophysical Research: Planets*, Vol. 128, No. 6, 2023. https://doi.org/10.1029/2022JE007474.

[3] Ellerby, D. T., and Gasch, M. J., "Heatshield for Extreme Entry Environment Technology (HEEET) Thermal Protection System (TPS)," *Annual Conference on Composites, Materials, and Structures*, 2019.

[4] Hollis, B., "Blunt-body Entry Vehicle Aerothermodynamics: Transition and Turbulence on the CEV and MSL Configurations," *40th Fluid Dynamics Conference and Exhibit*, AIAA Paper 2010-4984, 2010. https://doi.org/10.2514/6.2010-4984.

[5] Berger, K. T., Hollingsworth, K. E., Wright, S. A., and Rufer, S. J., "NASA Langley Aerothermodynamics Laboratory: Hypersonic Testing Capabilities," *53rd AIAA Aerospace Sciences Meeting*, AIAA Paper 2015-1337, 2015. https://doi.org/10.2514/6.2015-1337.

[6] Cheatwood, J., Johnston, C. O., and Hollis, B. R., "Mars Sample Return Earth Entry System Woven Roughness Mach 6 Aeroheating Test," *AIAA SciTech 2024 Forum*, AIAA Paper 2024-0443, 2024. https://doi.org/10.2514/6.2024-0443.

[7] Dahm, T., Cooper, L., Rafinejad, D., Youngblood, S., and Kelly, J., "Passive Nosetip Technology (PANT II) Program," *Vol. I., Rept. SAMS0-TR-77-11, Aerotherm, Acurex Corporation, Mountain View, California*, 1976.

[8] Hollis, B. R., Berger, K. T., Berry, S. A., Brauckmann, G. J., Buck, G. M., DiFulvio, M., Horvath, T. J., Liechty, D. S., Merski, N. R., Murphy, K. J., et al., "Entry, Descent and Landing Aerothermodynamics: NASA Langley Experimental Capabilities and Contributions," *52nd Aerospace Sciences Meeting*, AIAA Paper 2014-1154, 2014. https://doi.org/10.2514/6.2014-1154.

[9] Fay, J. A., and Riddell, F. R., "Theory of Stagnation Point Heat Transfer in Dissociated Air," *Journal of the Aeronautical Sciences*, Vol. 25, No. 2, 1958, pp. 73–85. https://doi.org/10.2514/8.7517.

[10] Merski, N. R., "Global Aeroheating Wind-Tunnel Measurements Using Improved Two-Color Phosphor Thermography Method," *Journal of Spacecraft and Rockets*, Vol. 36, No. 2, 1999, pp. 160–170. https://doi.org/10.2514/2.3446.

[11] Mason, M. L., and Rufer, S. J., "Imaging for Hypersonic Experimental Aeroheating Testing (IHEAT) Version 4.0: User Manual," Tech. Rep. NASA TM-2018-220113, November 2018.

[12] Cheatwood, J., "The Patch Integral Method (PIM), a New Heat Transfer Analysis Tool for Hypersonic Wind Tunnel Facilities at NASA Langley," Master's thesis, Virginia Polytechnic Institute and State University, 2023.

[13] Crank, J., and Nicolson, P., "A Practical Method for Numerical Evaluation of Solutions of Partial Differential Equations of the Heat-Conduction Type," *Proceedings of the Cambridge Philosophical Society*, Vol. 43, No. 1, 1947, pp. 50–67. https://doi.org/10.1017/S0305004100023197.

[14] Gonzalez, R. C., and Woods, R. E., *Digital Image Processing*, 3rd ed., Prentice Hall, Upper Saddle River, NJ, USA, 2008.

[15] Buhmann, M. D., *Radial Basis Functions: Theory and Implementations*, Cambridge University Press, 2003.

[16] Hollis, B. R., "Hexcomb-Pattern Roughness Effects on Blunt-Body Transition and Heating," *Journal of Spacecraft and Rockets*, Vol. 58, No. 6, 2021, pp. 1612–1635. https://doi.org/10.2514/1.A34791.

[17] Winovich, W., and WCA, C., "The 60-MW Shuttle Interaction Heating Facility," *Journal of Spacecraft and Rockets*, Vol. 19, No. 2, 1980, pp. 75–93.

[18] Hollis, B. R., "Distributed Roughness Effects on Blunt-Body Transition and Turbulent Heating," *52nd Aerospace Sciences Meeting*, AIAA Paper 2014-0238, 2014. https://doi.org/10.2514/6.2014-0238.

[19] Thompson, K. B., Hollis, B. R., Johnston, C. O., Kleb, B., Lessard, V. R., and Mazaheri, A., "LAURA Users Manual: 5.6," Tech. Rep. NASA TM-2020-220021, February 2020.

[20] Palmer, G., Johnston, C., Naughton, C., Liechty, D., and White, T., "An Overview of the Aerothermodynamic Database for the Mars Sample Return Earth Entry Vehicle," *20th International Planetary Probe Workshop (IPPW) 2023*, 2023.

[21] Cebeci, T., *Turbulence Models and Their Application: Efficient Numerical Methods with Computer Programs*, Springer Science & Business Media, 2003.

[22] Mazaheri, A., Johnston, C., and Palmer, G., "Progress Toward Evaluating Roughness-Resolved Aerothermodynamic Simulations for the Mars Sample Return Earth Entry System," *2nd International Conference on Flight Vehicles, Aerothermodynamics and Re-entry Missions & Engineering (FAR)*, 2022.